ELSEVIER

Journal of Chromatography A, 907 (2001) 57–71

JOURNAL OF CHROMATOGRAPHY A

www.elsevier.com/locate/chroma

Determination of the pore connectivity and pore size distribution and pore spatial distribution of porous chromatographic particles from nitrogen sorption measurements and pore network modelling theory

J.J. Meyers, S. Nahar, D.K. Ludlow, A.I. Liapis*

Department of Chemical Engineering and Biochemical Processing Institute, University of Missouri-Rolla, Rolla, MO 65409-1230, USA

Received 29 June 2000; received in revised form 4 October 2000; accepted 6 October 2000

Abstract

The pore connectivity, pore size distribution and pore spatial distribution of the porous structure of native and silanized silica particles were determined by matching the experimental nitrogen sorption data with the theoretical results obtained from pore network model simulations. The agreement between theory and experiment is found to be good. The results clearly indicate that the deposition of the silane layer to the pore surfaces of the native silica particles produces a silanized silica particle with a mean pore diameter and pore connectivity smaller than that of the native silica particle. Furthermore, the evaluation of the pore diffusivity of ribonuclease under unretained conditions shows that the lower values of the pore connectivity found in the samples of silanized silica particles, when compared with the values of the pore connectivity obtained for the native silica particles, increase the diffusional mass transfer resistance within the porous structure of the silanized silica particles.

Keywords: Pore connectivity; Pore size distribution; Pore spatial distribution; Pore network modelling theory; Nitrogen sorption; Silica particles; Stationary phases, LC

1. Introduction

The characterization of the physical structure of porous particles or monoliths employed in chromatographic systems represents an important step in the design, construction, evaluation and selection of chromatographic particles in order to maximize column performance. Meyers and Liapis [1,2], Liapis et al. [3], Liapis and Grimes [4], Grimes et al. [5] and Meyers et al. [6] have constructed and solved three-dimensional pore network models that can describe quantitatively the mass transfer and sorption mechanisms occurring in porous adsorbent particles or monoliths packed in columns whose flowing fluid stream is either pressure-driven (high-performance liquid chromatography (HPLC)) or electroosmotically-driven (capillary electrochromatography (CEC)); the pore size distribution of the particles could be monodisperse or bidisperse [1–6]. Their results [1–6] have shown that the dynamic (unsteady state) and steady-state behavior of the intraparticle diffusional and convective mass transport mechanisms, as well as the dynamic performance of the

*Corresponding author. Tel.: +1-573-341-4416; fax: +1-314-965-9329.

0021-9673/01/$ – see front matter
PII: S0021-9673(00)01018-9

chromatographic column depend greatly on the pore structure of the particles. The pore structure is characterized by the (i) pore size distribution, (ii) pore connectivity, n_T, of the pores, and (iii) the degree of randomness of the spatial distribution of the pores [1–7], while the values of the parameters that characterize the intraparticle pore diffusion and fluid flow of an adsorbate (solute) in the pore structure of the particles depend on items (i)–(iii) above as well as on (a) steric hindrance at the entrance to the pores, (b) frictional resistance within the pores, (c) molecular size of the adsorbate, (d) molecular size of the active sites (adsorption sites) immobilized on the surface of the pores, and (e) the fractional saturation (loading) of the adsorption sites [1–6].

Experimental methods for obtaining certain forms of information [1,2,8–16] about the pore structure of porous chromatographic packings include microscopic techniques such as small angle X-ray scattering, transmission electron microscopy (TEM), scanning electron microscopy (SEM), and neutron scattering, as well as invasive or penetrating methods such as mercury intrusion and extrusion, size exclusion chromatography (SEC), and nitrogen adsorption and desorption; Meyers and Liapis [1,2], Liapis et al. [3], and Unger [8] have indicated that experimental data obtained from a combination of these techniques would be necessary in order to accurately characterize porous media through the employment of three-dimensional pore networks [1–6]. Current laboratory apparatuses for mercury intrusion and extrusion and nitrogen adsorption and desorption, attempt to extract pore structure parameters for a given sample of porous particles by utilizing a parallel pore model to describe the porous structure of the porous particles; but the parallel pore model assumes that the value of the pore connectivity, n_T, of the pores is infinite and this contradicts the experimental evidence about the structures of real porous media which are found to have finite pore connectivities [1–3,9–16], and furthermore, the parallel pore model provides no information about the degree of randomness of the spatial distribution of the pores. The hysteresis between the nitrogen adsorption and desorption data is mainly due to the finite pore connectivity, n_T, of the pores of the porous particles [9,17] and the hysteresis can be viewed as a percolation process [1–6,9–16] where the sharpness of the desorption curve is caused by a vapor phase which percolates the lattice of pores. During the adsorption phase all pores have access to the condensing vapor and each pore can be treated as an individual pore that fills at its particular radius whereas during the desorption phase the pore connectivity of the pores has a significant effect because the condensed liquid must be available to the vapor phase in order to desorb [9,17].

In this work, the porous structures of porous silica particles is studied by comparing the experimental nitrogen adsorption and desorption data with the theoretical results obtained from pore network model simulations. Two different types of silica particles are examined: native silica and native silica with a silane layer of adsorption sites on the surface of the pores.

2. Experimental system and procedures

The porous silica particles employed in the experiments of this work were provided by Unger (private communication, 1999). Two types of porous silica particles were examined as discussed above: (i) native silica particles; and (ii) silanized silica particles. The particle size distribution for both types of particles is very narrow and their average particle diameter is about 3.5 μm. The surface coverage has 18.6% carbon content and the type of silanization is *n*-octadecyl dimethyl monochlorosilane; similar particles had been employed in CEC studies performed by Lüdtke [18]. The nitrogen adsorption and desorption experiments employing these particles were performed using the static volumetric method with an Autosorb-1C gas adsorption instrument (Quantachrome Corporation, Boynton Beach, Florida, USA). The samples of the particles were carefully weighed (to the ten-thousandth of a gram) and outgassed on the instrument at 300°C under high vacuum for a time period of 8–12 h to ensure that most of the free water bonded to the surface of the pores of the particles was removed; after the outgassing step, the samples were re-weighed to determine their dry weight and were prepared for analysis. The weight of each sample is reported in Table 2.

The instrument operates by first evacuating the sample cell to a pressure less than 10^{-5} Torr. The dead space volume, the volume in the sample cell not occupied by the sample, is determined by filling the apparatus' manifold with helium to a fixed pressure. The valve separating the manifold from the sample cell is then opened and the pressure drop monitored until it stabilizes. Since the pressure, temperature and volume of the manifold are accurately known before and after the volume expansion, the dead space volume can be determined. It is assumed that a negligible amount of helium adsorbs on the sample at room temperature. The sample cell is then re-evacuated and immersed in a liquid nitrogen bath and a second helium expansion is performed to determine the fraction of the sample cell located in the liquid nitrogen bath. The bath maintains the sample temperature at a constant 77.35 K, which is well below nitrogen's critical temperature of about 126 K. As the liquid nitrogen slowly evaporates, the dewar is raised automatically to maintain a constant level by using a thermistor as a sensor.

In order to obtain the equilibrium adsorption data, the manifold of the apparatus is filled with nitrogen gas to a fixed pressure and the valve separating the manifold from the sample cell is then opened and the pressure drop is monitored until it stabilizes; since the pressure, temperature and volume of the manifold and sample cell are known before and after the volume expansion, the difference between the calculated and measured pressure is attributed to adsorption of nitrogen gas onto the adsorbent particles. At the completion of an adsorption or desorption step, the atmospheric pressure, P_0, is measured. This ''dosing'' procedure continues until the prescribed pressure is reached and the pressure change is within prescribed tolerances. During desorption the above process is reversed, and therefore, in the desorption process the manifold pressure is maintained lower than the pressure of the sample cell. The instrument was connected to a computer running a software for data acquisition and analysis (Autosorb 1 for Windows, version 1.19) developed by Quantachrome Corporation. The software used the BJH [19] model (parallel pore model) for the complete range of pore diameters and the micropore analysis utilizes the expressions in Refs. [20,21].

The mesopore analyses on the samples consisted of a total of 145 points obtained over a P/P_0 range of 0.025–0.995 for the adsorption isotherm, and a range of 0.995–0.025 for the desorption equilibrium data. The points were evenly distributed for both the adsorption and desorption runs; intervals of 0.025 were considered in the range of P/P_0 from 0.025 to 0.6, while the interval is reduced to 0.008 for P/P_0 in the range from 0.6 to 0.995 to ensure maximum precision in the hysteresis region of the adsorption and desorption isotherms. The micropore analysis procedure was similar to that of the mesopore analysis except for the relative pressure range. The micropore analysis consisted of a total of 62 points obtained over a P/P_0 adsorption range of 10^{-6}–0.15. The main source of error within the instrument was from the transducers, and while this error varies with the range of pressure the average value of this error is considered to be about $\pm 0.11\%$.

3. Model formulation

In this work, both the contributions from the multilayer adsorption of nitrogen on the surfaces of the pores of the particle and capillary condensation within the pores are taken into account. The pressure of nitrogen vapor in the system is related to the pore radius by the sum of Kelvin's and de Boer's equations [22,23]. Kelvin's equation relates the relative pressure of nitrogen to the Kelvin radius, r_k (the radius of the section of the pore filled with capillary condensate), by the expression

$$r_k = \frac{-2 \times 10^8 \gamma V_m}{RT \ln\left(\frac{P}{P_0}\right)} \quad (1)$$

where γ represents the surface tension of nitrogen at its boiling point (8.85 ergs/cm^2 at 77 K), V_m is the molar volume of liquid nitrogen (34.7 cm^3/mol), T denotes the boiling point of nitrogen (77 K), R is the universal gas constant (8.314×10^7 ergs/deg/mol), P_0 is the reference (atmospheric) pressure (Torr), P represents the pressure of nitrogen vapor in the void space of the sample (Torr), and r_k (Å) denotes the Kelvin radius at P/P_0. de Boer's equation relates the relative pressure of nitrogen to the thickness, t, of the

adsorbed layer on the surface of the pores and is given by the expression

$$t = \left[\frac{13.99}{\log\left(\frac{P_0}{P}\right) + 0.034} \right]^{1/2} \quad (2)$$

where t (Å) represents the thickness of the adsorbed layer of nitrogen at P/P_0. Thus, the critical pore diameter, d_p^*, at a given relative pressure, P/P_0, of nitrogen is obtained from Eq. (3)

$$d_p^* = 2(r_k + t) \quad (3)$$

where the values of r_k and t are determined from Eqs. (1) and (2), respectively. The critical diameter, d_p^*, represents the pore diameter at which condensation occurs for a single isolated pore at a particular critical relative pressure P/P_0.

During adsorption, all the pores in the porous particles of the sample whose diameter is larger than the diameter of the nitrogen molecule, are accessible to the penetrating nitrogen vapor irrespective of the connectedness or arrangement of the pores [9,17]. Therefore, the nitrogen within each pore condenses at a critical pressure corresponding to the diameter of that particular pore ($d_p^* = d_p$), which in effect is the same as treating the entire void space within the sample of porous particles as a discrete collection of pores arranged in parallel [9,17]. For relative pressures, P/P_0, less than d_p^*, nitrogen adsorbs on the surface of empty pores (those not filled with capillary condensate) with a thickness given by Eq. (2). This continues with increasing steps of relative pressure, P/P_0, until a relative pressure is reached such that the critical diameter, d_p^*, equals the diameter, d_p, of a particular pore. In this case, the remaining open portion of the pore is filled with capillary condensate. The BJH method [19] considers that all pores within the sample are accessible, during adsorption, irrespective of the connectedness or arrangement of the pores (the BJH method [19] employs a parallel pore model), and therefore, the BJH method is used to obtain a pore size distribution (PSD) of the pores in the sample from the equilibrium adsorption isotherm of nitrogen [19]. Thus, the BJH method [19] determines over a relative pressure increment the volume, V_p, of pores of radius, r_p, and calculates the PSD by dividing V_p at each relative pressure increment by the corresponding volume of one pore ($\pi r_p^2 l_p = 2\pi r_p^3$)considering the pore length, l_p, to be equal to its diameter ($l_p = 2r_p$).

During desorption, Kelvin's and de Boer's equations are used to relate the relative pressure of nitrogen to the pore diameter. Since a pore must be exposed to the vapor phase in order to evacuate its capillary condensate and desorb nitrogen, pore network effects slow the desorption behavior observed for a sample of porous particles. Pore shadowing (a large pore whose pathway to the vapor phase is blocked by a smaller pore) causes the nitrogen in a pore not to desorb at its corresponding critical pore diameter but to be dependent on the desorption of other pores. Therefore, during desorption the connectedness or arrangement of the pores [9,17] plays a very significant role and, thus, a pore network arrangement [1–6] of pores is employed to describe nitrogen desorption behavior. The sample of porous particles is topologically mapped onto a cubic lattice network of interconnected cylindrical pores and the lattice employed in our work has a regular array of nodes (the lattice size L is the same along the x, y, and z space coordinates of the network, and thus, $x \times y \times z{:}L \times L \times L$) that are connected to each other by bonds (pores) of the pore network. The pore connectivity, n_T, denotes the number of pores connected to a node of the pore network. The porous structure in the sample of porous particles has (a) interstitial pores which represent the pores between the particles of the sample and which contain the bulk nitrogen vapor, and (b) intraparticle pores which represent the pores within the porous particles. The nodes of the cubic lattice are considered to have no volume while the bonds (pores) of the pore network are considered to provide the pore volume of the network. The pore network (model porous medium) is constructed by randomly assigning cylindrical pores to the bonds of the cubic network with the distribution of the size of pore diameters being chosen in a representative manner from the pore size distribution (PSD) extracted using the BJH method. The bond (pore) length, l_p, used in the construction of the lattice network can be related to the pore diameter, d_p, and can either be randomly assigned or constant [1,2]. Dullien [24] reports that various photomicrographic investigations indicate that the length, l_p, of a pore is of the same order of

magnitude as its diameter, d_p. In this work, the pore length, l_p, is taken to be equal to the diameter of the pore, d_p, since network simulations of porous media [1,2,15,25,26] have shown that network model predictions for mass transfer parameters based on all of the various methods used to assign pore lengths, agree well with experimental data. In our pore network model, the pore length, l_p, could be assigned in any of the above mentioned methods, and the assignment of l_p, to be equal to d_p in this work, is considered to be topologically reasonable in light of the findings of the above mentioned researchers [1,2,15,24–26]. In the pore volume of the sample, the interstitial and intraparticle pores are correlated [1,2,15,27] and, thus, cannot be assigned to the network randomly. Therefore, in order to generate a realistic model of the porous medium (network) representation of the pore volume of the sample, the interstitial pores are assigned [1,2,15,28] in a semi-random manner to a percolating cluster that transects the lattice. The assignment of the intraparticle pores in the network is completely random. It should be noted here that there could exist certain porous chromatographic particles in which the macropores (or the mesopores) are not randomly distributed relative to the micropores (non-random bidisperse pore network); in such a case, our approach in constructing the intraparticle pore network is slightly modified by employing in the assignment of the intraparticle pores the procedures developed by Meyers and Liapis [1,2], Petropoulos et al. [7], and Petrou et al. [29].

The experimental equilibrium desorption data of nitrogen are compared with the theoretical results obtained from the pore network model and the best fit between the theoretical and experimental results provides the value of the pore connectivity, n_T, and the degree of randomness of the spatial distribution of the pores.

4. Results and discussion

In this work, experimental nitrogen sorption measurements were obtained for three samples of porous native silica particles and for three samples of porous silanized silica particles. The three samples of native silica particles are labelled as Rsil1-2, Rsil1-4, and Rsil1-5, while the three samples of silanized silica particles are labelled Ssil2-1, Ssil2-2, and Ssil2-4. Both types of particles have a very narrow particle size distribution and their average particle diameter is about 3.5 μm; similar particles had been employed in CEC studies performed by Lüdtke [18]. The silica particles are from the same batch and the bonded silicas are manufactured from the Rsil (native silica) particles.

In Figs. 1–6, the pore volume fraction and pore number fraction of the native and silanized silica samples are presented. The pore size distribution results in Figs. 1–6 were obtained from the application of the BJH method [19] or from the application of the parallel pore network model (model porous medium of infinite pore connectivity) simulation of Meyers [30] on the experimental [31] equilibrium

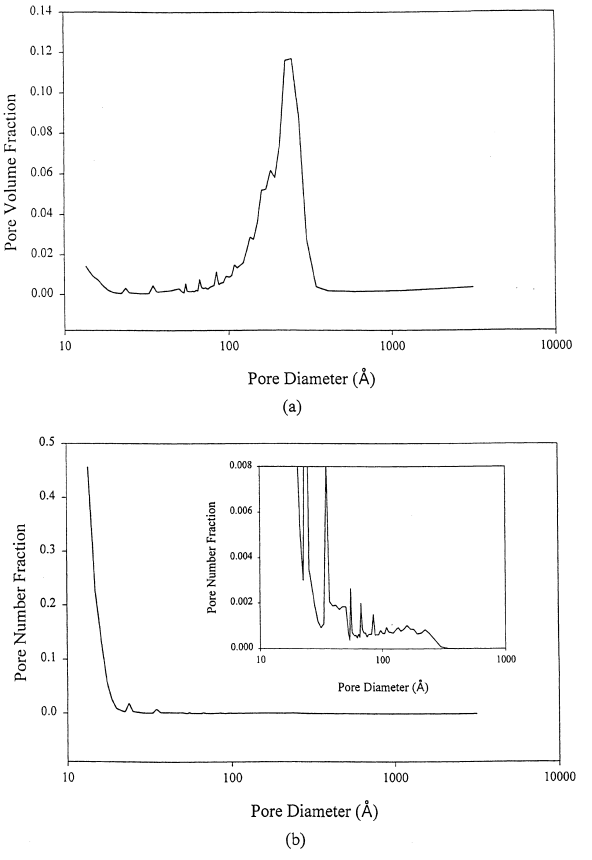

Fig. 1. Pore volume fraction (a) and pore number fraction (b) distributions for the porous native silica particles of sample Rsil1-2.

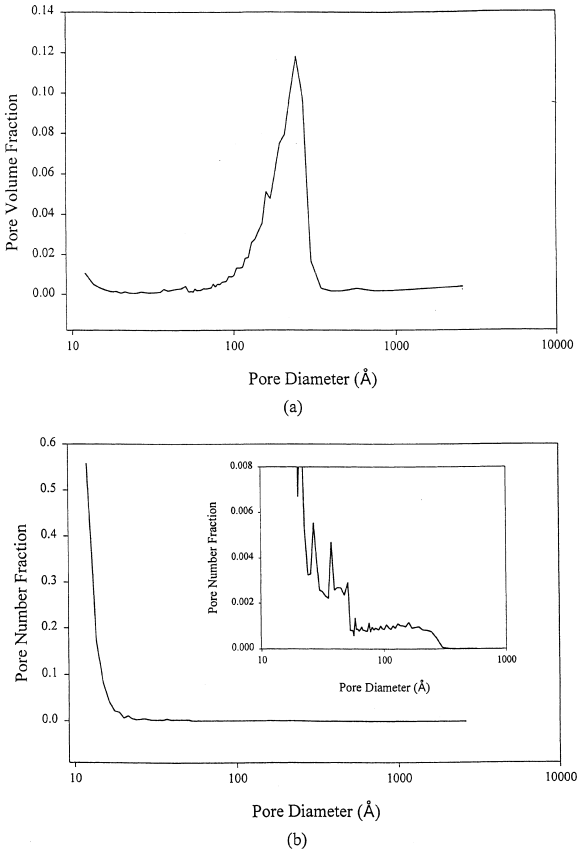

Fig. 2. Pore volume fraction (a) and pore number fraction (b) distributions for the porous native silica particles of sample Rsil1-4.

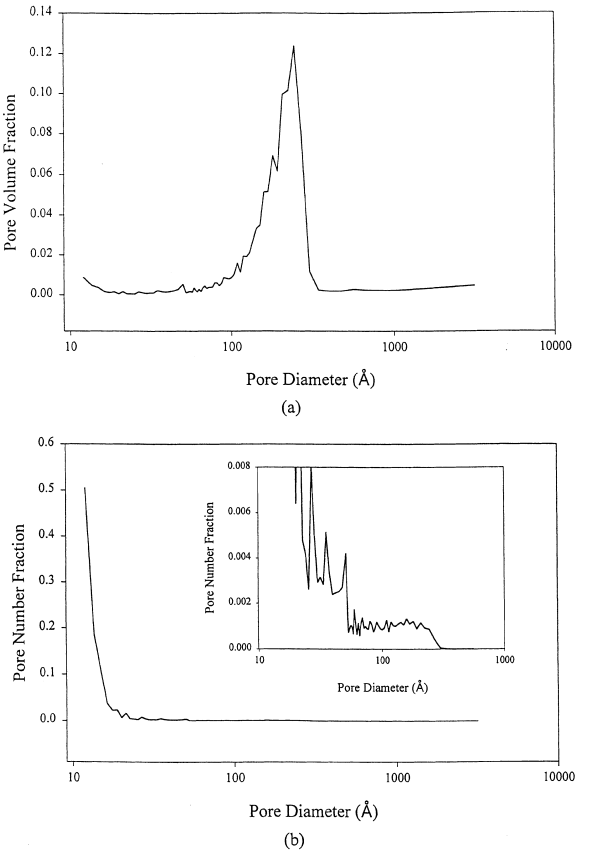

Fig. 3. Pore volume fraction (a) and pore number fraction (b) distributions for the porous native silica particles of sample Rsil1-5.

adsorption data of nitrogen; both the BJH method [19] and the parallel pore network model of Meyers [30] provide, from the experimental adsorption data of nitrogen, identical pore size distributions. Part (a) in each of the Figs. 1–6 provides the pore volume fraction at a particular pore diameter; the pore volume fraction is obtained by dividing the amount of pore volume determined from the BJH method [19] or the parallel pore network model of Meyers [30] (at a particular pore diameter) by the total pore volume. Part (b) in each of the Figs. 1–6 provides the number of pores of a particular diameter divided by the total number of pores (pore number fraction); the inset in part (b) for each of the Figs. 1–6 provides a more detailed representation of the pore number fraction showing the large discrepancy between the relative amounts of micropores (microvoids) and mesopores. The results in Part (b) for each of the Figs. 1–6 are obtained from the results presented in Part (a) of each figure, by dividing each pore volume obtained by the BJH method [19] or the parallel pore network model of Meyers [30] by the volume of a cylindrical pore of length, l_p, equal to its diameter, d_p, at the corresponding pore diameter ($(\pi/4)d_p^3$). In Table 1, the values of the specific surface area and specific pore volume of the native and silanized silica particles are presented. These values have been determined by considering pore diameters up to about 430 Å. The results in Table 1 clearly show that the silanization process reduced significantly the specific surface area and specific pore volume of the native porous silica particles.

The pore size distribution (PSD) results in Figs. 1–6 show that although the majority of the pore

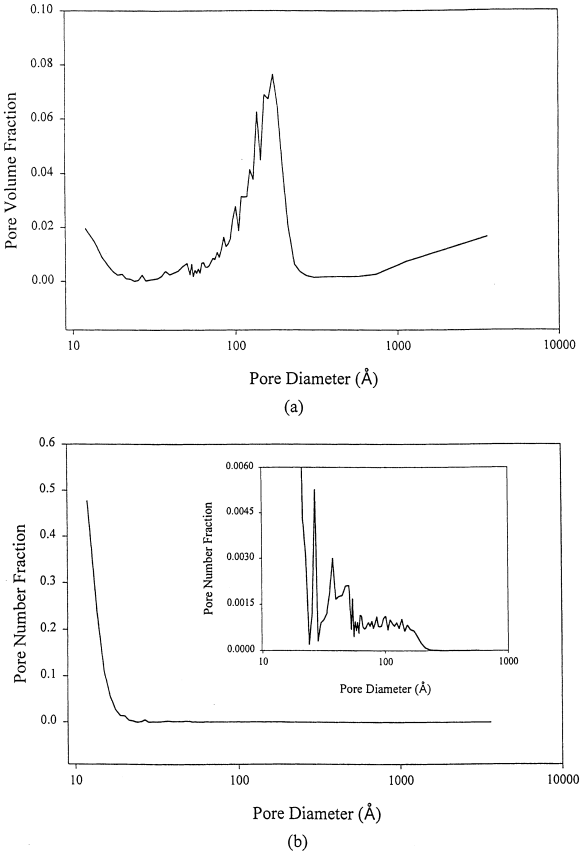

Fig. 4. Pore volume fraction (a) and pore number fraction (b) distributions for the porous silanized silica particles of sample Ssil2-1.

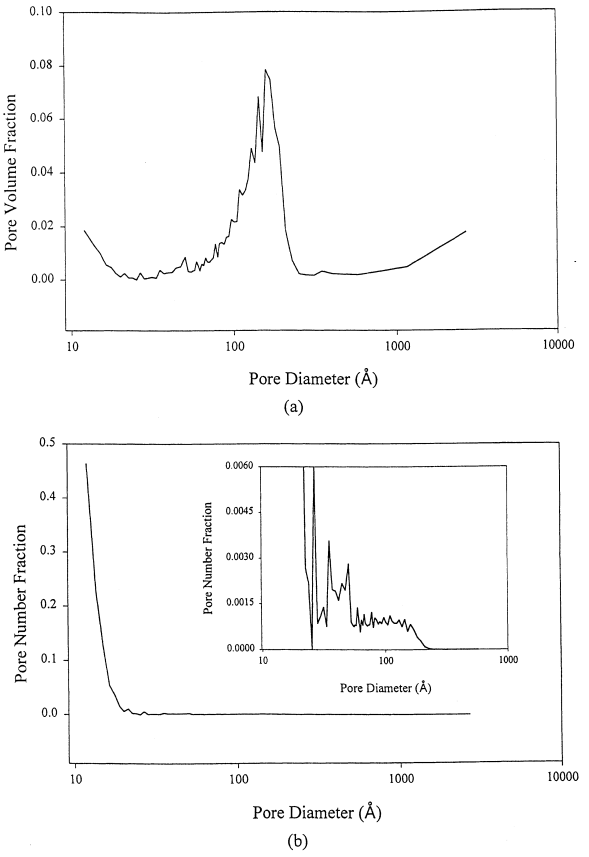

Fig. 5. Pore volume fraction (a) and pore number fraction (b) distributions for the porous silanized silica particles of sample Ssil2-2.

volume is located in the mesopore diameter range of 20–500 Å, the number of small pores in the diameter range of 10–20 Å contributes nearly 90% of the total number of pores in each sample. Table 2 presents the mean and standard deviation determined from the results given in Part (b) of each figure; these values were obtained from the PSD over the entire range of pore diameters in each distribution. The reason the values of the mean and standard deviation calculated using Part (a) of each figure are not presented is that these values based on the pore volume fraction are not useful in the construction of the pore network model. The mean and standard deviation based on the pore volume fraction do not provide proper information as to the topology of the structure of the porous particles that will have to be represented by a pore network model since, in the formulation of network modelling, the volume of the porous medium is represented on a per pore basis. It can be observed from Table 2 that the deposition of the silane (SiO_2^-) layer to the pore surfaces of the native silica particles produces a silanized silica particle with a mean pore diameter slightly smaller than that of the native silica particle. This is in agreement with what was physically expected to occur, since the silane group, although small, restricts the size of the pore in such a way as to reduce the mean pore size. From the data in Table 2, it can also be observed that the standard deviation of the PSD decreases from the deposition of the silane layer. Thus, since the mean pore diameter decreased while the size of adsorbate (nitrogen) molecule (which could be considered to indicate the size of the minimum pore diameter at which adsorption could occur) remained constant in

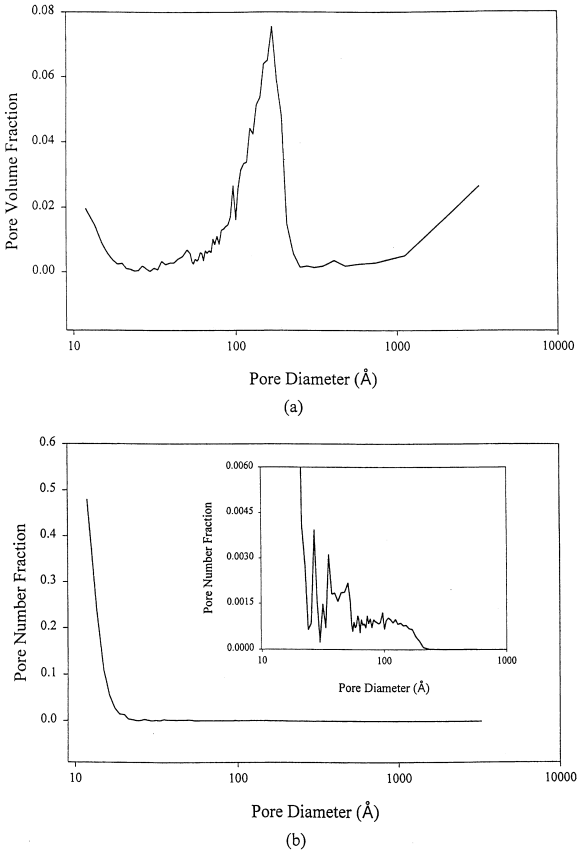

Fig. 6. Pore volume fraction (a) and pore number fraction (b) distributions for the porous silanized silica particles of sample Ssil2-4.

value, the width of the PSD decreased as a direct result of the deposition of the silane layer. By comparing the pore volume fraction for the samples of native silica (Part (a) in Figs. 1–3) with the pore volume fraction for the samples of silanized silica (Part (a) in Figs. 4–6), it becomes apparent that the amount of pore volume attributed to pores of diameter greater than 1000 Å increases upon silanization. This is misleading in the sense that silanization most likely affects the size of the smaller pores within the sample to a higher degree, thereby reducing the amount of pore volume in pores of diameter less than 1000 Å to a larger extent than those larger than 1000 Å pores. This decrease in total pore volume, mainly contributed to by the pores of diameter less than 1000 Å, makes the relative amount of pore volume of the pores of diameter greater than 1000 Å to contain a larger fraction of the total pore volume; it is worth noticing the decrease in the value of the peak in the pore volume fraction between the native and silanized silica samples. Furthermore, from the results in Figs. 1–6 it can be observed that the amount of volume attributed to pores of diameter less than 20 Å increases upon silanization, but only slightly. Although the value of the pore number fraction at the smallest pore diameter is larger for the native silica particles than the silanized silica particles, the width of this region of the pore number fraction (spanning the lowest pore diameter to an appropriate cutoff diameter chosen at the approximate minimum of the pore number fraction) displays a larger percentage of pores for the silanized sample than for the native. The reason for having more pores of diameter less than 20 Å in the silanized silica particles is due to the fact that by silanizing the native silica particles, not only are more pores made into small pores, but more small cracks and crevices for adsorption of nitrogen are produced between the

Table 1
Values of the specific surface area and specific pore volume of the native and silanized silica particles

Sample type	Sample name	Specific surface area (m^2/g)	Specific pore volume (cm^3/g)
Native silica	Rsil1-2	361.33	1.277
Native silica	Rsil1-4	352.24	1.221
Native silica	Rsil1-5	358.43	1.251
Silanized silica	Ssil2-1	169.92	0.579
Silanized silica	Ssil2-2	180.23	0.609
Silanized Silica	Ssil2-4	178.30	0.606

Table 2
Mean and standard deviation of the pore size distributions presented in part (b) of Figs. 1–6 for the entire range of the pore diameters in each distribution

Sample type	Sample name	Sample weight (g)	Mean pore diameter (Å)	Standard deviation (Å)
Native silica	Rsil1-2	0.0106	18.62	0.1922
Native silica	Rsil1-4	0.0385	17.65	0.2089
Native silica	Rsil1-5	0.0265	18.44	0.2207
Silanized silica	Ssil2-1	0.0378	16.43	0.1548
Silanized silica	Ssil2-2	0.0333	16.69	0.1575
Silanized silica	Ssil2-4	0.0372	16.44	0.1553

silane molecules attached to the surfaces of larger pores. It is worth also mentioning here that by the addition of the silane layer on the surface of the pores of the native silica particles, some of the smallest pores of the native silica particles could become too small with respect to the size of the nitrogen molecules, and therefore, such small pores could not allow nitrogen adsorption and would effectively be blocked. Despite this possibility, the increased width of this region produces a larger number of microvoids for the silanized silica particles.

Unger [8] indicates that the accurate range for the Kelvin equation is between the pore diameters of 20–500 Å (the mesoporous range) while Mason [9–11] considers that the Kelvin equation is applicable in the relative pressure, P/P_0, range of 0.5–1.0 corresponding to pores of diameter greater than 30 Å. While the BJH method [8,19] is not accurate in the range of diameters that correspond to micropores, micropore analyses [31] performed on these samples by using the experimental adsorption data and the micropore analysis expressions of Saito and Foley [21] show that indeed a peak in pore volume is found in the range of pores of diameter 5–20 Å. Therefore, the large peak in pore number fraction at small pore diameters, as calculated by the BJH method, was included as true pore volume in the pore network model simulations of the desorption of nitrogen.

In the construction of the pore network model (model porous medium) for the analysis of the experimental equilibrium desorption data of nitrogen, it is considered conceptually not very realistic to have void spaces of less than 20 Å in diameter to be part of an intersecting network of pores with an associated pore connectivity because of their extremely small size; it is even difficult to label these as ''pores'' because of their size. The large peak in pore number observed at small values of the pore diameter in the pore number fraction distribution of each sample (Figs. 1–6), was considered to arise from imperfections and irregularities on the pore surface of the pores of the particles. Because of this consideration, it was taken that the physical system of void spaces in the porous silica particles (native and silanized) could be modeled as an intersecting pore network of mesopores to which a relative number of microvoid diameters (in a representative distribution equal to the total microvoid distribution) are assigned in a parallel pore structure. Therefore, although the microvoids are in a parallel pore structure, they cannot begin to desorb until their ''parent'' mesopore, which is part of an intersecting network of mesopores, desorbs. This relative number of the total number of microvoids per the total number of mesopores, $n_{\mathrm{micro/meso}}$, can be determined from the normalized pore number fraction of the total sample and is calculated from Eq. (4)

$$n_{\mathrm{micro/meso}} = \frac{1}{\sum_{i=d_c}^{\infty} PSD(i)} - 1 \tag{4}$$

where $PSD(i)$ represents the value of the pore number fraction distribution at pore diameter i, and d_c denotes the cutoff diameter between which microvoids and mesopores are distinguished. Since only the mesopores are arranged in an intersecting pore network, the number of mesopores, n_{meso}, is defined by the pore connectivity, n_T, and lattice size, L, of the network. The total number of pores in the pore network is determined by Eq. (5)

$$n_{\mathrm{total}} = n_{\mathrm{meso}} + (n_{\mathrm{meso}} \cdot n_{\mathrm{micro/meso}}) \tag{5}$$

The number of mesopores, $N_{\mathrm{diam,meso}}(i)$, of a specific pore diameter, $d_{\mathrm{p,i}}$, is then determined from expression (6)

$$N_{\mathrm{diam,meso}}(i) = n_{\mathrm{micro/meso}} \left(\frac{PSD(i)}{\sum_{i=d_c}^{\infty} PSD(i)} \right)$$

$$\text{for } i = d_c,\ldots,\infty \tag{6}$$

for the mesoporous range, and $\Sigma_{i=d_c}^{\infty} N_{\mathrm{diam,meso}}$ provides the total number of mesopores in the pore network model. The number of microvoids per mesopore, $N_{\mathrm{diam,micro/meso}}(i)$, of a particular pore diameter, $d_{\mathrm{p,i}}$, is then obtained from Eq. (7)

$$N_{\mathrm{diam,micro/meso}}(i) = n_{\mathrm{micro/meso}} \left(\frac{PSD(i)}{\sum_{i=0}^{d_c} PSD(i)} \right)$$

$$\text{for } i = 0,\ldots,d_c \tag{7}$$

Because the BJH method [19], and therefore, the Kelvin and de Boer equations were used for the full

range of relative pressures, P/P_0, in extracting from the equilibrium nitrogen adsorption data the pore size distributions presented in Figs. 1–6, it was considered necessary to employ Kelvin's and de Boer's equations also for the analysis of the equilibrium nitrogen desorption data in order to obtain a total pore volume consistent with that determined from the analysis of the adsorption data by the BJH method [19].

The experimental equilibrium nitrogen desorption data were fitted utilizing the pore number fraction distributions in Part (b) of Figs. 1–6 and by considering different values for the pore network model parameters consisting of the pore connectivity, $n_{T,}$ of the mesopores, the lattice size, L, of the pore network, and the degree of randomness in the spatial distribution of the mesopores. The values of the parameters that provide the best fit between the experimental desorption data and the theoretical results obtained from the pore network model employed in this work, as well as the values of the correlation coefficient, R, between the simulated and experimental desorption curves, are shown in Table 3, with the corresponding comparisons plotted in Figs. 7–12. It should be noted here that the pore connectivity, n_T, reported in Table 3 is for the pore network of mesopores, and does not include the microvoids attached to each mesopore in a parallel pore arrangement. Therefore, when discussing the size of pores as related to pore network effects, it is the relative numbers of mesopores that is referred to. The largest micropore for each sample type was chosen at a pore diameter where the minimum pore number fraction was encountered in Part (b) of each

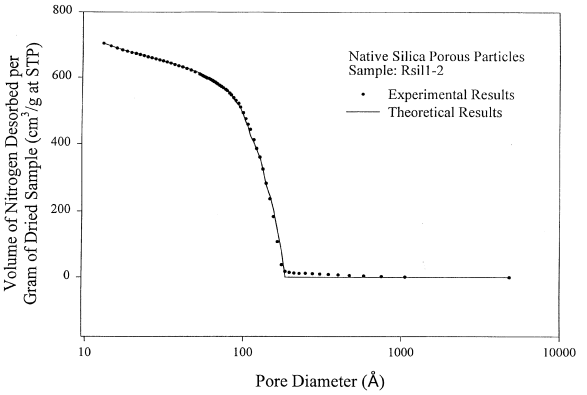

Fig. 7. Experimental and theoretical results of the volume of nitrogen desorbed per gram of dried sample (cm^3/g at STP) at different pore diameters for the porous native silica particles of sample Rsil1-2.

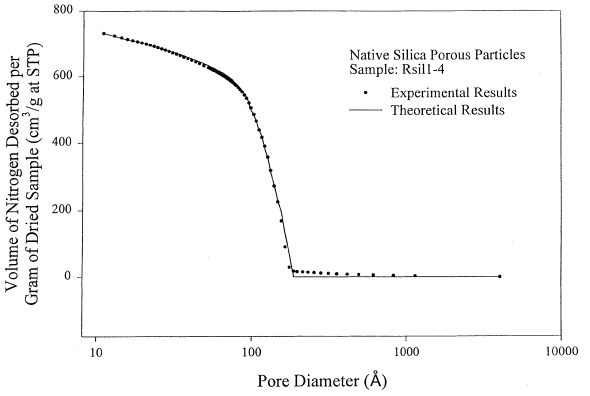

Fig. 8. Experimental and theoretical results of the volume of nitrogen desorbed per gram of dried sample (cm^3/g at STP) at different pore diameters for the porous native silica particles of sample Rsil1-4.

Table 3
Pore network model parameters determined by matching the experimental nitrogen desorption data with the theoretical results obtained from pore network model simulations

Sample type	Sample name	Lattice size, L	Pore connectivity, n_T	Pore spatial distribution (Å)	Largest micropore (Microvoid) Diameter (Å)	Correlation coefficient, R, that provides the degree of goodness of agreement between the experimental nitrogen desportion data and the theoretical results
Native silica	Rsil1-2	5	11.00	non-random, 150.0<Surface<181.0	20.5	0.99944
Native silica	Rsil1-4	5	10.00	non-random, 150.0<Surface<180.0	20.5	0.99937
Native silica	Rsil1-5	5	11.00	non-random, 150.0<Surface<179.0	20.5	0.99937
Silanized silica	Ssil2-1	5	6.00	non-random, 130.0<Surface<142.0	22.0	0.99753
Silanized silica	Ssil2-2	5	6.40	non-random, 130.0<Surface<142.0	22.0	0.99740
Silanized silica	Ssil2-4	5	6.00	non-random, 130.0<Surface<142.0	22.0	0.99685

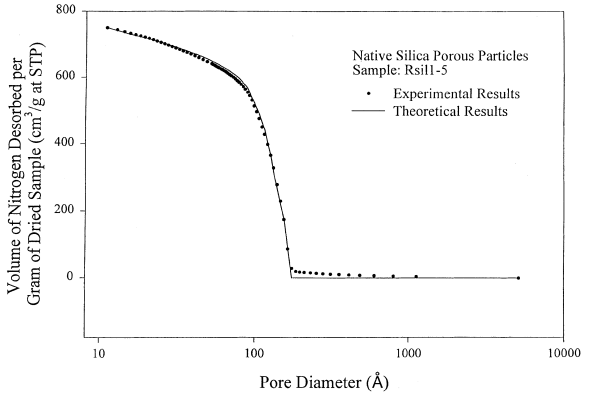

Fig. 9. Experimental and theoretical results of the volume of nitrogen desorbed per gram of dried sample (cm^3/g at STP) at different pore diameters for the porous native silica particles of sample Rsil1-5.

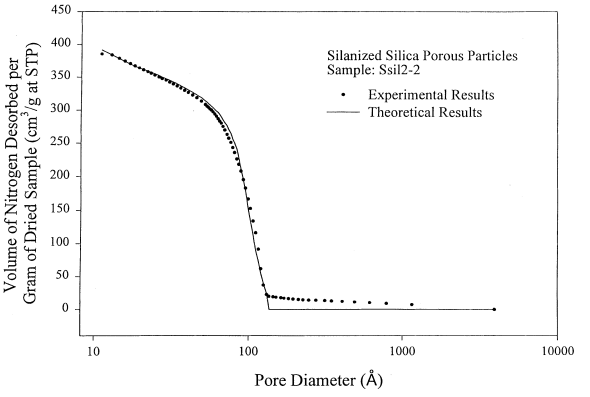

Fig. 11. Experimental and theoretical results of the volume of nitrogen desorbed per gram of dried sample (cm^3/g at STP) at different pore diameters for the porous silanized silica particles of sample Ssil2-2.

figure. The lattice size that produced the best fit in all cases was small, $L=5$. The small size of these lattices could be a consequence of the fact that the shapes of the experimental equilibrium adsorption and desorption curves are relatively identical (although shifted) and that the adsorption curve is fitted with an infinitely connected (parallel pore model) medium employed by the BJH method. The combination of these two facts may predispose the best fit arrangement (for desorption) to be a pore network with a small amount of network effects. This is the case for small lattices since all pores are closer to the surface of the network and, therefore, a shorter path length exists for the desorption of the nitrogen from the pores. The pore connectivity, n_T, used to fit the data does decrease from the native silica particles to the silanized silica particles, and this is consistent with the theoretical consideration that by adding the silane layer, not only are the sizes of the pores of the native silica are decreased, but the complete blockage of some of the very small pores results in a decrease in the pore connectivity, n_T, thereby reducing the number of alternative pathways within the porous particles. By restricting the number of alternative pathways for desorption, the amount of pore shadowing is increased and the pore connectivity of

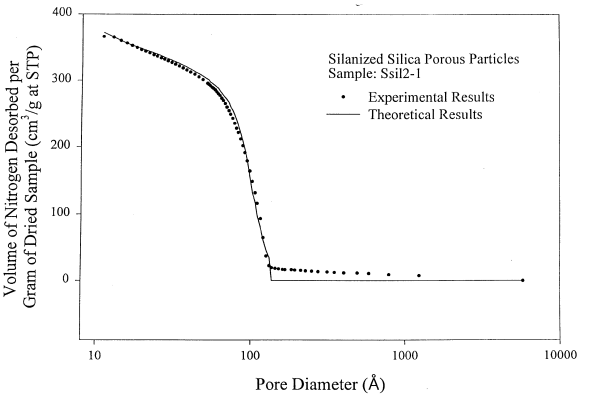

Fig. 10. Experimental and theoretical results of the volume of nitrogen desorbed per gram of dried sample (cm^3/g at STP) at different pore diameters for the porous silanized silica particles of sample Ssil2-1.

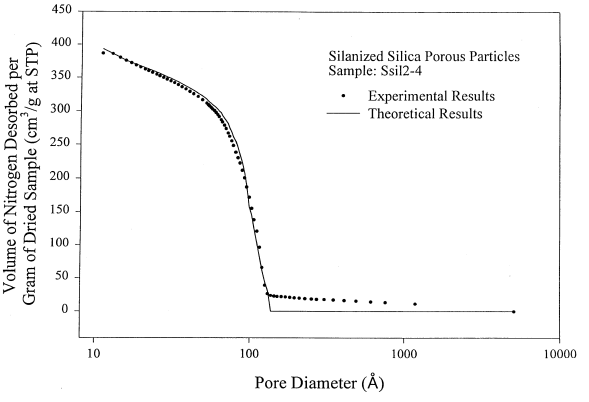

Fig. 12. Experimental and theoretical results of the volume of nitrogen desorbed per gram of dried sample (cm^3/g at STP) at different pore diameters for the porous silanized silica particles of sample Ssil2-4.

the porous medium appears to be reduced. A comparison of the slopes of the experimental desorption curves between the native and silanized silica samples also indicates that the amount of pore shadowing has increased from the native to the silanized silica samples since the slope of the desorption curve for the silanized silica samples is less than those of the native silica samples, indicating a larger amount of pore shadowing in the silanized silica samples.

Furthermore, in each case, a pore spatial distribution was considered that limited the diameter of pores that could be placed on the surface of particles; this was necessary because completely random pore spatial distributions could not provide [30] a good agreement between the experimental nitrogen desorption data and the theoretical results obtained from pore network model simulations. A range of pore diameters was considered that were systematically restricted to sites directly connected to the external surfaces of the model porous medium (including interstitial pore axis, and top and bottom surfaces [1–3,5,6]), thereby randomly placing pores with diameters larger and smaller than this range in the interior of the pore network. This non-random pore spatial distribution approximated well the shift observed between the equilibrium adsorption and desorption curves of each sample of particles. By employing this procedure, a very accurate fit is obtained for the desorption data of nitrogen from the samples of native silica particles, as observed by the values of the correlation coefficient, *R*, reported in Table 3.

Because of the apparent larger amount of pore volume at large pore diameters for the samples of silanized silica particles, the fit was not very satisfactory in this region of pore diameters. It was postulated that possibly by placing a few larger pores on the surface of the pore network, while still restricting the majority of the surface pores to a specific range of pore diameters, this might provide a more adequate fit of the data for the samples of silanized silica particles. It was determined that in order to obtain a representative set of pore diameters that provided the necessary number of large pores to be reflected in this pore diameter range, a large lattice needed to be selected. This also hints at the observation that this initial increase in the amount of desorbed volume is more of a macroscopic characteristic of the porous sample. Additional fits were attempted with larger lattice sizes in an attempt to obtain a better agreement between the experimental desorption data and the simulated results for the silanized silica particles at large pore diameters. It was found that for a lattice of size $L = 40$ and pore connectivity $n_T = 10$ where a certain number of the large pores were placed on the surface of the model porous medium, the simulated results of the desorption of nitrogen from the pores increased slowly at high pore diameters similar to the experimental values, but then increased very rapidly once a percolative cluster of vapor phase was encountered. The sharpness of this desorption front in these simulations was more than that observed in the experimental data, sacrificing the agreement between the experimental and simulated desorption results in the region of small pore diameters, despite a number of trials with different pore connectivities and pore spatial distributions; the value of the correlation coefficient, *R*, for this network was 0.99073. Therefore, it can be considered that the previously obtained small lattices ($L = 5$) adequately represent the interior (more microscopic) regions of the porous silanized particles containing the great majority of the surface area accessible for adsorption, while the larger network ($L = 40$) provides a fit on a more macroscopic scale. Direct comparison or linkage of the two types of pore networks into one equivalent network is not possible since the values of lattice size, *L*, and pore connectivity, n_T, are interrelated. By examining the values of the correlation coefficient, *R*, for the samples of silanized silica in Table 3, it is indicated that the theoretical results obtained from the pore network models having a lattice size $L = 5$ are in good agreement with the experimental desorption data for the overall range of pore diameters.

Pore diffusion simulations were also performed using the pore modeling theory of Meyers and Liapis [1,2] in order to determine the ratio of the pore diffusion coefficients of a solute determined from (i) the pore network model employing the pore number fraction distributions in Figs. 1–6 and the pore connectivity, n_T, values and pore spatial distributions shown in Table 3, and (ii) the parallel pore model (the parallel pore model considers that the magnitude of the pore connectivity, n_T, is infinite, that is all

pores in the porous particles are connected with each other) employing the pore number fraction distributions in Figs. 1–6; it is worth mentioning again here that the BJH method [19] employs a parallel pore model. The pore diffusivity of ribonuclease (bovine pancreas) was determined in the pores of the native and silanized silica particles studied in this work. The molecular diameter, α_1, of ribonuclease is 32.8 Å and its free molecular diffusion coefficient, D_{mf}, is 1.31×10^{-6} cm^2/s. In the calculations for determining [1,2] the pore diffusivities $D_{p,network\ model}$ and $D_{p,parallel\ pore\ model}$ of ribonuclease which correspond to the pore diffusivities obtained from the pore network model and parallel pore model, respectively, the values of the porosities of the native and silanized silica particles used in these calculations were 0.58 and 0.43, respectively. The value of the porosity of the void space formed by the packed spherical particles in each sample was taken to be 0.36 because such a value of bed porosity for these particles had been determined (Unger (private communication, 1999)) experimentally. Since the average particle diameter for these particles is about 3.5 μm, a value of 1.05 μm was considered to be reasonable for the diameter of the channels (pores) in the void space formed by the particles packed in the sample (the value of 1.05 μm provides a fraction of (1.05 μm/3.5 μm)=0.3, which agrees well with previous work [1,2,24]). In Table 4, the values of the ratios $D_{p,\ parallel\ pore\ model}/D_{mf}$ and $D_{p,\ network\ model}/D_{mf}$ clearly indicated that the diffusion of ribonuclease in the pores of the native and silanized silica particles is highly restricted [1–3]. This is mainly due to the fact that the molecular diameter, α_1 ($\alpha_1 = 32.8$ Å), of ribonuclease is nearly of the same order of magnitude as most of the pore diameters in the porous native and silanized silica particles. By comparing the values of the ratios $D_{p,\ parallel\ pore\ model}/D_{mf}$ and $D_{p,\ network\ model}/D_{mf}$ for the native and silanized silica particles it becomes apparent that the silanized silica particles restricted the pore diffusion of ribonuclease more than the native silica particles. Furthermore, it can be observed in Table 4 that the values of the ratio $D_{p,\ network\ model}/D_{p,\ parallel\ pore\ model}$ are small, signifying that the mass transfer resistance within the pore network model is significantly higher than the mass transfer resistance in the parallel pore model. It is also observed that the values of the ratio $D_{p,\ network\ model}/D_{p,\ parallel\ pore\ model}$ are smaller for the silanized silica particles than those of the native silica particles, and these results clearly indicate that the lower values of the pore connectivity, n_T, found in the samples of the silanized silica particles increase the magnitude of the diffusional resistance within these particles. Finally, the results in Table 4 strongly indicate that the pore diffusivities in chromatographic particles should be determined from pore network models and not from the physically unrealistic parallel pore model.

5. Conclusions and remarks

In this work, the pore size distribution, the pore connectivity, and the pore spatial distribution of the porous structure of native and silanized silica particles were determined by matching the experimental nitrogen sorption measurements with the theoretical results obtained from pore network model simula-

Table 4
Values of the ratios of the pore diffusion coefficient of ribonuclease determined from the parallel pore model ($D_{p,\ parallel\ pore\ model}$) and the pore network model ($D_{p,\ network\ model}$), respectively, to the free molecular diffusion coefficient, D_{mf} ($D_{mf}=1.31\times10^{-6}$ cm^2/s), of ribonuclease, as well as values of the ratio $D_{p,\ network\ model}/D_{p,\ parallel\ pore\ model}$

Sample type	Sample name	$D_{p,\ parallel\ pore\ model}/D_{mf}$	$D_{p,network\ model}/D_{mf}$	$D_{p,\ network\ model}/D_{p,\ parallel\ pore\ model}$
Native silica	Rsil1-2	9.1736×10^{-4}	8.6599×10^{-5}	0.0944
Native silica	Rsil1-4	8.9338×10^{-4}	9.4162×10^{-5}	0.1054
Native silica	Rsil1-5	9.3040×10^{-4}	10.5221×10^{-5}	0.1131
Silanized silica	Ssil2-1	6.2376×10^{-4}	5.4579×10^{-5}	0.0875
Silanized silica	Ssil2-2	6.1412×10^{-4}	5.2936×10^{-5}	0.0862
Silanized silica	Ssil2-4	6.1946×10^{-4}	5.6122×10^{-5}	0.0906

tions. The agreement between theory and experiment was found to be good.

The results clearly indicate that the deposition of the silane layer to the pore surfaces of the native silica particles produces a silanized silica particle with a mean pore diameter and pore connectivity smaller than that of the native silica particle. The capability of the pore network model in determining the structural changes that occurred in the porous structure of the native silica particles after the deposition of the silane layer on the surface of their pores, indicates that pore network modeling theory should be employed in the determination and evaluation of the porous structure of chromatographic particles before and after the deposition of a chemical layer that provides desirable adsorption sites.

Finally, the pore network model and the parallel pore model were used to determine the pore diffusivity of ribonuclease under unretained conditions in the pores of the native and silanized silica particles. The ratio of the pore diffusivity obtained from the pore network model to the pore diffusivity determined from the parallel pore model, is small and indicates that the mass transfer resistance within the pore network model porous medium is significantly higher than the mass transfer resistance in the parallel pore porous medium of the same cross-section. Furthermore, the ratios are smaller for the silanized silica particles than those of the native silica particles, and indicate that the lower values of the pore connectivity found in the samples of the silanized silica particles increase the diffusional mass transfer resistance within these particles. The pore diffusion results clearly show that the value of the pore diffusivity of a solute in chromatographic particles should be determined from pore network models [1–7] and not from the physically unrealistic parallel pore model.

Acknowledgements

The authors are grateful to Professor K.K. Unger and Dr. S. Lüdtke of the Institut für Anorganische Chemie und Analytische Chemie of Johannes Gutenberg-Universität, Mainz, Germany, for providing the samples of the porous native and silanized silica particles used in this work. The authors also gratefully acknowledge support of this work by Monsanto and the University of Missouri Research Board.

References

[1] J.J. Meyers, A.I. Liapis, J. Chromatogr. A 827 (1998) 197.
[2] J.J. Meyers, A.I. Liapis, J. Chromatogr. A 852 (1999) 3.
[3] A.I. Liapis, J.J. Meyers, O.K. Crosser, J. Chromatogr. A 865 (1999) 13.
[4] A.I. Liapis, B.A. Grimes, J. Chromatogr. A 877 (2000) 181.
[5] B.A. Grimes, J.J. Meyers, A.I. Liapis, J. Chromatogr. A 890 (2000) 61.
[6] J.J. Meyers, O.K. Crosser, A.I. Liapis, J. Chromatogr. A (2001), in press.
[7] J.H. Petropoulos, J.K. Petrou, A.I. Liapis, Ind. Eng. Chem. Res. 30 (1991) 1281.
[8] K.K. Unger, Chromatographic Sciences Series, in: K.K. Unger (Ed.), Packings and Stationary Phases in Chromatographic Techniques, Vol. 47, Marcel Dekker, New York, 1990, p. 43.
[9] G. Mason, J. Colloid. Interf. Sci. 88 (1) (1982) 36.
[10] G. Mason, Proc. R. Soc. London, Ser. A 390 (1983) 47.
[11] G. Mason, Proc. R. Soc. London, Ser. A 415 (1988) 453.
[12] N.A. Seaton, Chem. Eng. Sci. 46 (1991) 1895.
[13] H. Liu, L. Zhang, N.A. Seaton, Chem. Eng. Sci. 47 (1992) 4393.
[14] P. Rajniak, R.T. Yang, AIChE J. 39 (5) (1993) 774.
[15] K.C. Loh, D.I.C. Wang, J. Chromatogr. A 718 (1995) 239.
[16] P. Rajniak, M. Soòs, R.T. Yang, AIChE J. 45 (4) (1999) 735.
[17] J.J. Meyers, Internal Report Number 55, Department of Chemical Engineering, University of Missouri-Rolla, Rolla, Missouri, 2000.
[18] S. Lüdtke, Ph.D. Dissertation, Institut für Anorganische Chemie und Analytische Chemie, Johannes Gutenberg-Universität, Mainz, Germany, 1999.
[19] E.P. Barett, L.G. Joyner, P.P. Halenda, J. Am. Chem. Soc. 73 (1951) 373.
[20] G. Horvath, K. Kawazoe, J. Chem. Eng. Jpn. 16 (1983) 470.
[21] A. Saito, H.C. Foley, AIChE J. 37 (1991) 429.
[22] D.H. Everett, Trans. Faraday Soc. 50 (1954) 1077.
[23] J.H. de Boer, in: D.H. Everett, F.S. Stone (Eds.), The Structure and Properties of Porous Materials, Butterworths, London, 1958, p. 68.
[24] F.A.L. Dullien, Porous Media: Fluid Transport and Pore Structure, 2nd ed., Academic Press, New York, 1992.
[25] A.O. Imdakm, M. Sahimi, Chem. Eng. Sci. 46 (1991) 1977.
[26] S.D. Rege, H.S. Fogler, Chem. Eng. Sci. 42 (1987) 1553.
[27] M.P. Hollewand, L.F. Gladden, Chem. Eng. Sci. 47 (1992) 1761.
[28] J.J. Meyers, Internal Report Number 12, Department of Chemical Engineering, University of Missouri-Rolla, Rolla, Missouri, 1998.

[29] J.K. Petrou, J.H. Petropoulos, N.K. Kanellopoulos, A.I. Liapis, in: A.B. Mersmann, S.E. Scholl (Eds.), Proceedings of the Third International Conference on Fundamentals of Adsorption, Engineering Foundation, New York, 1990, p. 679.

[30] J.J. Meyers, Ph.D. Dissertation, Department of Chemical Engineering, University of Missouri-Rolla, Rolla, Missouri, 2000.

[31] S. Nahar, M.S. Thesis, Department of Chemical Engineering, University of Missouri-Rolla, Rolla, Missouri, 2000.